Verification/validation and physics model extension in high fidelity 3D RF full wave simulations on Petra-M

Verification/validation and physics model extension in high fidelity 3D RF full wave simulations on Petra-M

S. Shiraiwa,[1, a)] N. Bertelli,[1] R. Bilato,[2] P. Bonoli,[3] W. Helou,[4] J. Hillairet,[5] C. Lau,[6] E. Martin,[6] D. Milanesio,[7] J. Myra,[8] W. Tierens,[2] J. C. Wright,[3] and RF SciDAC

[1]*Princeton Plasma Physics Laboratory, Princeton, NJ, USA.*
[2]*Max-Planck-Institut für Plasmaphysik, Boltzmannstrasse 2,D-85748 Garching, Germany*
[3]*Massachusetts Institute of Technology, Cambridge, MA, USA*
[4]*ITER Organization, Route de Vinon-sur-Verdon, CS 90 046, 13067 St. Paul Lez Durance Cedex, France*
[5]*CEA, IRFM, F-13108 Saint-Paul-Lez-Durance, France*
[6]*Oak Ridge National Laboratory, TN 37830 Oak Ridge, USA*
[7]*Politecnico di Torino, Corso Duca degli Abruzzi, 24, 10129 Torino TO, Italia*
[8]*Lodestar Research Corporation, 5055 Chaparral Ct., Suite 102, Boulder, CO 80301, USA*

[a)]Corresponding author: shiraiwa@princeton.edu

Abstract. This paper reports the recent progress towards a whole-device scale RF actuator simulation. Our approach is to combine progresses made by open source scientific and math software communities for meshing, FEM assembly, and linear solvers to construct an integrated FEM fullwave simulation framework (the Petra-M FEM framework). The goal is to bring in engineering CAD level geometrical detail to our wave simulation capability, and advanced RF wave physics models, such as RF rectified sheath models and non-local hot plasma effects. In Petra-M, the high harmonic fast wave (HHFW) propagation was fully resolved in a 3D NSTX-U torus. In the NSTX-U simulation, the ratio between wavelength to the device size reaches ~ 15, which is in the range required for resolving the ICRF wave fields in ITER. Verification and validation of the RF wave field computed by Petra-M through the international/multi-institutional efforts has been a major research focus, which yields an excellent code benchmark agreement between Petra-M, TOPICA and RAPLCIASOL. The spectral analysis of 3D wave field has been performed to interrogate the wave field behavior, which shows the consistency with the wave theory. RF rectified potential model was incorporated in our wave field solver. We developed a new non-linear iteration algorithm, which allows for using both the thick sheath (asymptotic) model and non-linear sheath impedance models seamlessly. The 3D RF sheath simulation on the WEST ICRF antenna indicates that the sheath potential tends to concentrate near the corner of antenna box, which is consistent with experimental observation of RF induced heat load pattern.

INTRODUCTION

It is widely recognized that, through various fusion experiments, predicting an accurate RF actuator performance requires to understand mutually coupled physics processes which spread over a wide range of spatial and time scale. The eventual goal of our simulation model development is to realize an integrated RF actuator simulation in which the computational domain contains entire 3D torus plasmas, and accurate wave physics models and geometrical details are included.

FIGURE 1 (left) illustrates the physics ingredients, which are crucial for such high-fidelity RF simulations, and how they interact mutually. The red box in the figure indicates the physics processes that we treat in this paper. The central component is the wave electric field simulation, which can be viewed as being composed from two parts, the wave field in the core and the SOL regions. The wave is excited externally by an antenna/transmitter, propagates in the SOL, and then enters the plasma core. As discussed in [1], in the core and edge regions, the wave field tends to be governed by very different set of physics. In the core region, non-local conductivity is important in order to include finite temperature effects accurately, while the plasma shape has toroidal symmetry. In contrast, SOL regions including the antenna structure have complicated geometrical shape and lacks the toroidal symmetry, while the plasma response to the RF field can be treated a local response (no spatial dispersion) in the majority of computational domains. An important point is, however, that the wave fields in two regions are tightly coupled, and we need to solve the field self-consistently (arrow (1) in FIG. 1). Indeed, we proposed an accurate way to solve the core and edge regions together based on surface impedance matching [1]. For the present work, however, we use a cold plasma approximation with collisions in entire plasma regions, which allows for treating the core and edge regions as one piece.

The wave electric field interacts with other physics processes, often in a bi-directional manner. What we treat in this paper is the integration of the RF sheath physics (arrow (2) in FIG. 1). In the edge, an electron-depleted thin

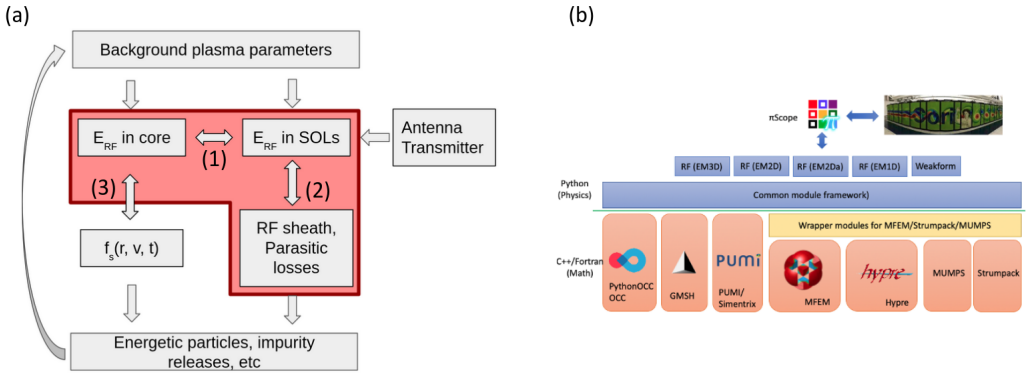

FIGURE 1. (a) Schematics of physics components for integrated RF actuator simulations, and (b) current code structure of the Petra-M FEM framework.

layer, called a sheath, is formed in front of the plasma facing components (PFCs). The non-linear I-V characteristic of the sheath rectifies the RF electric field and the resultant large DC electric field is important for understanding the impurity release during the ICRF operation. From the viewpoint of solving the Maxwell's equations, the sheath modifies the boundary condition on the computational boundary.

There are other important physics processes which needs to be integrated in wave field simulation, although we don't address them in the present work. One crucial process is the modification of the particle distribution function due to the RF quasilinear diffusion and the consequent change of plasma response to the RF electric field (arrow (3) in FIG. 1). The particle distribution function, the impurity release due to RF electric field rectification, and other physics processes such as the ponderomotive pressure due to a large antenna near field (See [2, 3] and this conference [4]) could impact the background plasma parameters, making the entire physics processes coupled together in a complicated manner.

In the past RF conferences, we reported the development of the Petra-M FEM framework [5, 6] based on open source software libraries. Petra-M is equipped with a user friendly GUI-driven interface, allowing for constructing a complicated RF simulation model coupled with different physics processes. We believe that a transparent access to the physics implementation is essential to achieve a rather complicated physics model integration. In the last few years, the framework grew significantly to become a fully integrated FEM analysis platform (FIG. 1 (right)), on which a user can complete a FEM simulation workflow from geometry and mesh preparation to solution visualization. Our present work focuses on the physics components and their connections shown in solid red block in the figure.

This paper is organized as follows. First, we discuss the recent development of the Petra-M framework and the resultant progress in resolving the RF wave field in a 3D torus. Next, we discuss how we verify and validate the computed wave fields. We perform in-depth code benchmarking through multi-institutional collaboration to compare Petra-M results with other RF antenna codes, such as RAPLICASOL [7, 8] and TOPICA [9, 10]. We also inspect the wave field spectrum and compare it with wave field theory. This reveals an interesting spectrum behavior, which is difficult to capture in 2D simulation. Then, we discuss our RF rectified potential model integration approach in 3D. There has been multiple new approaches proposed in order to incorporate the RF sheath in fullwave RF simulation relatively recently [11, 12, 13]. This paper focuses, however, what was implemented in Petra-M. Finally, we show an integrated RF rectified potential simulation on the WEST ICRF antenna limiters and summarize this paper.

PROGRESS IN 3D WAVE FIELD SOLVER AND SPECTRUM ANALYSIS

On a large device, the average RF wavelength, λ, compared to the device size tends to become small ($\lambda/R \sim$ 10-20 on ITER), and resolving such a wave field in 3D space accurately is computationally expensive. FIGURE 2 compares the HHFW wave field simulation in a 3D NSTX-U torus computed by Petra-M shown at the previous conference [6] and a more recent one. One can immediately see that the wavelength in the torus is much shorter in the recent simulation, and in fact, the wavelength qualitatively agrees with 2D simulations (not shown), where we can actually confirm the convergence of the wave field using order/mesh refinement methods. The improvement illustrated in FIGURE 2 was made possible thanks to the advancements in the underling libraries we are using. For example, the recent simulation

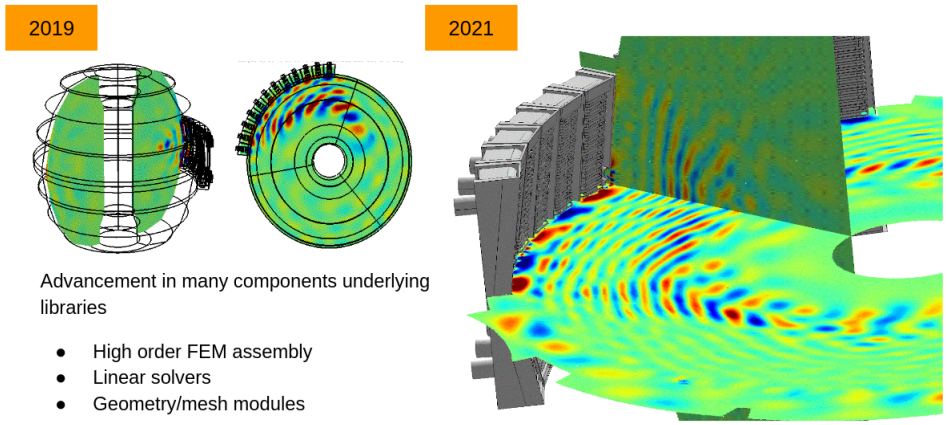

FIGURE 2. Progress in 3D HHFW wave field simulation based on the slide presented at 24th topical conference of RF power in plasmas.

uses 4-th order H(curl) finite element basis function, instead of linear elements. Multi-frontal direct solvers (MUMPS [14] is used in this case) are continuously improving their memory and arithmetic operation efficiency, allowing for solving a large relatively dense (compared to a low order element) FEM system matrix. One can also see that the antenna geometry is much more detailed in the recent simulation. This geometry is generated directly from a defeatured engineering CAD model using the new CAD module, which uses OpenCASCADE CAD library [15] and its Python wrapper (Python-OCC [16]). Further detail of the NSTX-U simulations can be found in Ref. [17].

As shown in FIGURE 2, the wave electric field computed in the 3D torus is rather complicated. Therefore, it has been a challenge to interrogate this wave field to confirm that the wave physics is implemented correctly and identify if and how 3D geometric effects manifest in results. What we found useful for this purpose is the wave field spectrum analysis. We project the finite element solution represented on an unstructured mesh to a cylindrical (R-ϕ-Z) regular grid. Then, the field is Fourier transformed in the toroidal direction, yielding the toroidal spectrum on each R-Z grid point.

FIGURE 3 shows the toroidal spectrum evaluated on the torus mid-plane, as a function of the toroidal mode number, n_ϕ and the major radius, R. The left figure is the spectrum when the antenna phasing is 150 degree and the right figure is the spectrum when the antenna phasing is 30 degree. Near the antenna (at large R), the peak of spectrum intensity corresponds to the peaks anticipated from the antenna phasing. An important feature is that spectrum intensity is bounded by the curves that indicate the location of fast wave cut-off, determined by $k_{||}^2 = \frac{\omega^2}{c^2}(S+D)$. In other words, the wave field spectrum spreads only in the part of phase space where the wave is propagative.

In both cases shown in FIG. 3, we notice that there is the vertically straight pattern. This seems to suggest that the toroidal mode number is reasonably conserved in these simulations. Comparing this spectrum, however, with the spectrum computed with pure 2D simulation reveals that what is going on in these 3D wave field spectra is not that simple. FIGURE 5 (left) shows a spectrum obtained by post-processing the wave electric field computed from a 2D simulation, in which we stretched the plasma parameters on the mid-plane in the vertical direction (150 degree phasing is used). The 2D case exhibits the straight vertical pattern more clearly, having a more constant width. Furthermore, the evanescent high n_ϕ ($n_\phi > \sim 50$) components excited near the antenna do not propagate inward, but their intensity decays as it goes toward small R. Compared to 2D, the 3D spectrum seems more complicated. The difference may be most obvious when looking at $n_\phi \sim 0$ component in the 30 degree phasing case. In 3D, while the antenna is not exciting at $n_\phi \sim 0$, the spectrum intensity gets higher at $R \sim 0.4$.

It turns out that the wave spectrum $n_\phi \sim 0$ in the 3D simulations can be explained by looking at the same spectrum on the poloidal plane. FIGURE 4 shows the spectrum components at $n_\phi = 5$ and 1 from the 30 degree phasing simulation. On the left, $n_\phi = 5$ corresponds to the peak of the antenna spectrum. In this case, one can see that spectrum intensity in front of the antenna is uniform in the vertical direction. At this n_ϕ, the poloidal distribution of spectrum is similar to what is computed in a 2D simulation (FIG. 5 (right)). Therefore, we can say that the antenna is exciting the wave as it is designed and the wave propagates as predicted in the earlier works. What is interesting is the spectrum component at lower n_ϕ shown in FIG. 4 (right). In this case, the spectrum intensity is not vertically uniform in front of the antenna. Instead, it is small near the mid-plane and gets larger near the top and bottom part of the antenna. Then, the wave

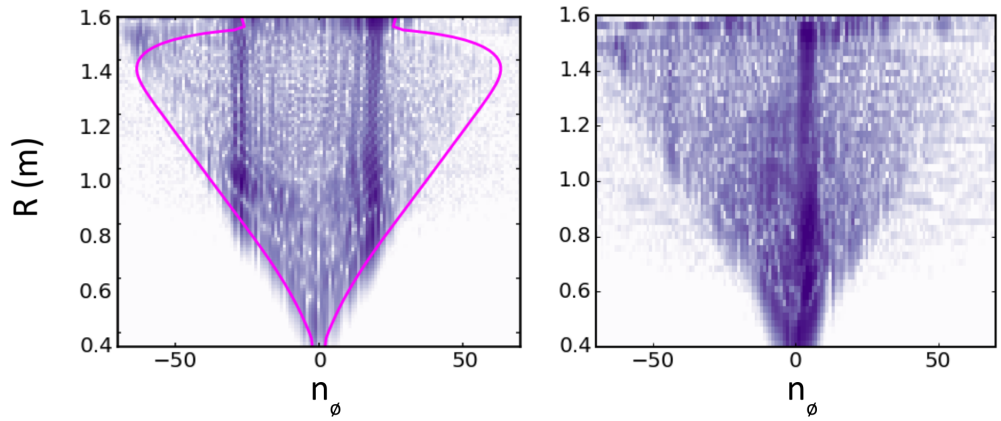

FIGURE 3. Mid-plane spectrum of NSTX-U 3D HHFW wave field. Antenna phasing of 150 deg. and 30 deg. are used in the left and right cases, respectively. See [17] for detailed plasma parameters used in these simulations.

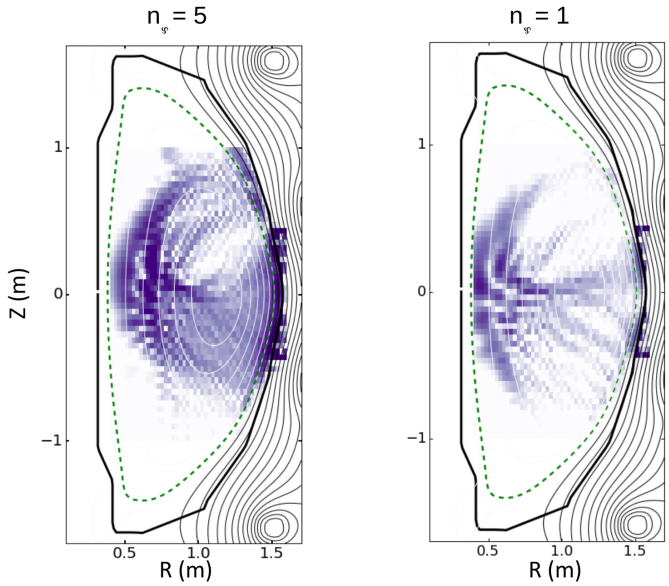

FIGURE 4. HHFW wave field spectrum on poloidal cross-section for n_ϕ = 5 (left) and 1 (right), respective. The sepctrum is computed from the 30 deg. antenna phasing case.

travels towards the mid-plane and then spreads vertically. Therefore, if we look at the mid-plane, the wave intensity is weak on the out-board side and it gets intensified as it goes towards the inboard side as pointed out earlier. This excitation/propagation pattern of low n_ϕ components is rather unexpected, and the image current on the antenna box is considered to be playing a role, thus it is unique to 3D wave field simulation. In the 3D simulation, very high ($> \sim 50$) n_ϕ components do not exhibit clear radial decay (evanescence) in front of the antenna. While we don't have a clear explanation for this yet, one possibility may be because the toroidal mode number is not conserved well near the antenna region due to the realistic 3D structure of antenna, which mixes the different toroidal modes.

VERIFICATION/VALIDATION OF 3D WAVE ELECTRIC FIELD

One of our research focus has been verifying and validating the computed 3D electric field. We benchmarked the 3D RF electric field computed by Petra-M with other well-established ICRF antenna codes (TOPICA and RAPLICA-SOL), and compared the parameters which characterize the antenna coupling including scattering matrix (S-matrix),

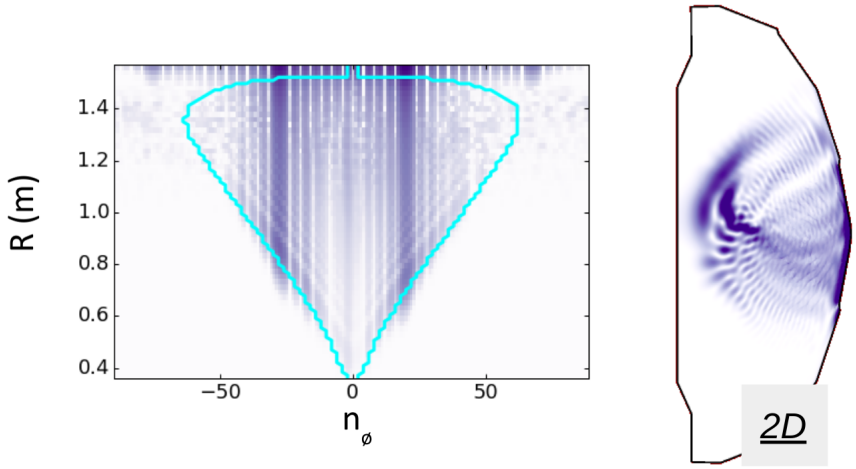

FIGURE 5. Wave field spectrum computed using 2D simulations. (Left) toroidal spectrum of 2D mid-plane simulation, where the plasma is stratified in the vertical direction. (Right) 2D axis-symmetric simulation using $n_\phi = 5$.

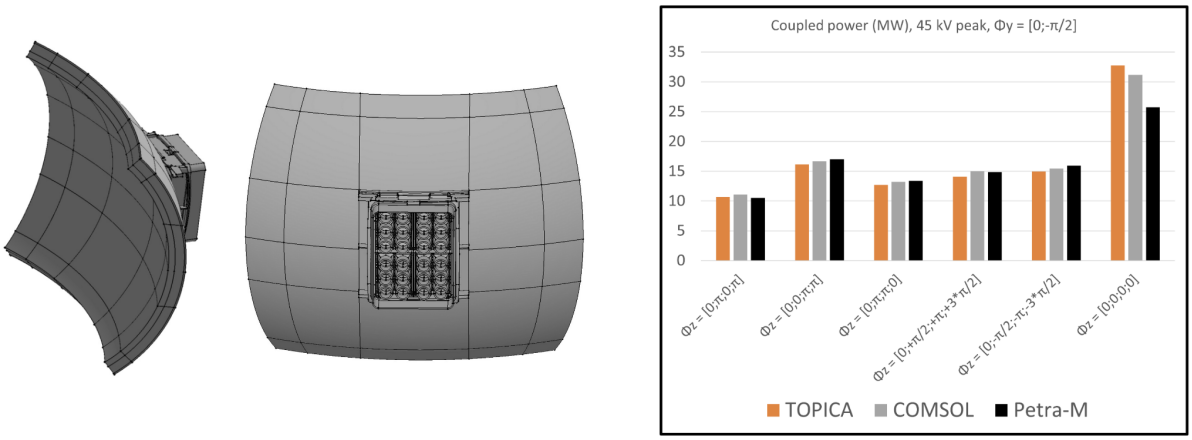

FIGURE 6. (Left) ITER antenna and plasma geometry used for the code benchmark between Petra-M, RAPLICASOL and TOPICA. (Right) comparison of ICRF coupled power predicted for various antenna excitation operational modes.

and antenna near field pattern. This was done by international collaborations on various tokamak devices including AUG [18], WEST [19], JET [20] and ITER [21]. Overall, an excellent agreement has been widely observed in terms of both antenna S-matrices and the RF electric field. As an example, FIGURE 6 shows the code comparison performed using an ITER ICRF antenna model. In this particular case, we used a so-called 24 port ITER ICRF geometry (shown in left of FIG. 6) [22, 23, 24], and we used an identical FEM mesh in COMSOL and Petra-M. FIGURE 6 (right) shows the comparison of coupled ICRF power, demonstrating a good agreement between three codes within a few % except for the mono-pole ([0,0,0,0]) phasing case, which tends to show a larger disagreement in general.

In parallel to the code benchmark activity, the code validation using experimental data is in progress. As an example, FIGURE 7 shows a simulation of the LH wave excitation from the LH1 launcher on the WEST tokamak [19]. The LH wave electric field parallel to the static magnetic field in front of the top waveguide row shows the resonant cone propagation in the forward and backward directions. The wave polarization ($\equiv \arctan(|E_z|/|E_r|)$) is also shown at several poloidal cross-sections. The LH1 launcher on WEST is equipped with the DSELF diagnostics [25], which measures the wave electric field intensity from the D_β spectrum (inset picture). On the right, a predicted diagnostic signal synthesized from the simulation data is shown. The direct comparison between these synthetic diagnostic signal with experimental data was discussed at this conference, and will be published in the near future.

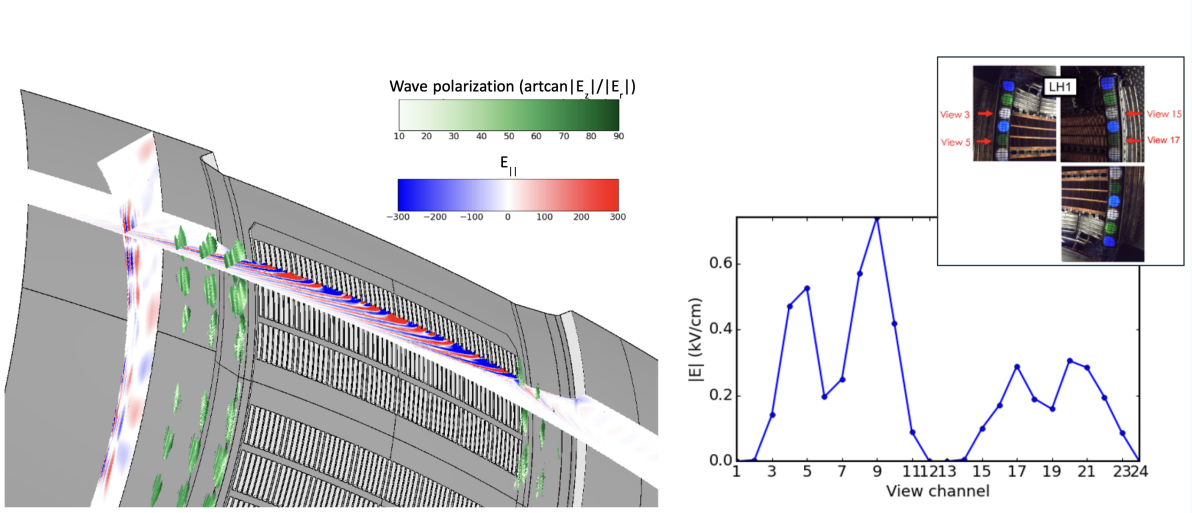

FIGURE 7. LH waves launched from the WEST LH1 antenna. (Left) the parallel (with respect to the static magnetic field) electric field (a.u.) and the wave polarization, (right) profile of the synthesized DSELF signal and DSELF diagnostic lines of sight are shown. The RF electric field shown on the left is scaled to match the total injected power with the experiment in order to compute the synthetic DSELF signal. Note that collision frequency is elevated towards the small R direction to create a radiative boundary.

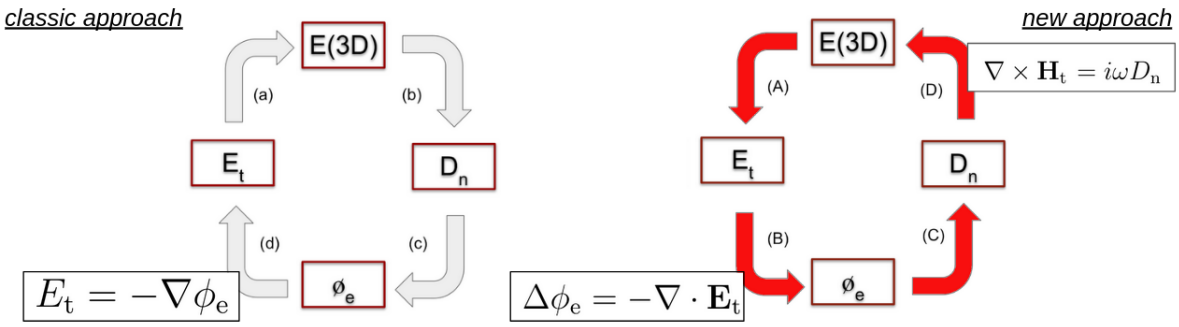

FIGURE 8. Iteration schemes for non-linear sheath simulation. (Left) classical approach computes the tangential electric field using a gradient of sheath potential. (Right) New approach computes the sheath potential from the tangential component of electric field.

INTEGRATED RF SHEATH BOUNDARY CONDITION MODEL

The formation of RF rectified potential (RF sheath) and resultant ion bombardment on plasma facing components (PFCs) is widely accepted as a key physics process causing the impurity increase during the ICRF operation. Because the RF sheath is physically very thin, a boundary condition (BC) model to represent the sheath effects using zero thickness surface was proposed ("RF sheath BC") [26]. Developing such a boundary condition and using it in global RF field full-wave simulation has attracted considerable attention in the RF theory and computational community [27, 28, 29, 30, 31, 32, 33, 34, 35]. Several authors noted, however, the difficulty of using an RF sheath model in a 3D full-wave simulation in the literature [26, 32, 35, 36]. In the RF SciDAC project, we developed alternative two approaches, both of which could potentially scale to a large non-linear 3D simulation [11, 12].

An approach we took in Petra-M [11] is to expand the finite element solution space with auxiliary scalar potentials for the magnetic fields on the plasma-sheath boundary. In a generalized sheath impedance model, the RF sheath BC can be expressed in the following coupled non-linear equations.

$$\mathbf{E}_t = -\nabla\phi_e \tag{1}$$

$$D_{\rm n} = -i\phi_{\rm e}/\omega z_{\rm sh}(|\phi_{\rm e}|), \tag{2}$$

where the first equation defines the tangential electric field on the plasma-sheath boundary as a gradient of sheath potential $\phi_{\rm e}$. The second equation gives the total current entering the plasma-sheath boundary, $i\omega D_{\rm n}$, as a function of sheath potential and sheath impedance, $z_{\rm sh}(|\phi_{\rm e}|)$. Since the sheath impedance is a function of sheath potential, the resultant coupled problem becomes non-linear. Thus, we seek a self-consistent set of global electric field (E) and physics quantities defined on plasma-sheath boundaries ($\mathbf{E}_{\rm t}$, $D_{\rm n}$, and $\phi_{\rm e}$), iteratively.

A standard approach in the literature to implement this non-linear iteration follows the above two equations in a literal sense as shown schematically in FIGURE 8(left). In Petra-M, we link E, $\mathbf{E}_{\rm t}$, $D_{\rm n}$, and $\phi_{\rm e}$ in the opposite direction as shown in FIGURE 8(right). It turned out that this new scheme provides more stable and faster convergence, compared to our earlier attempt to implement the classic approach in Petra-M. A key point of this approach is that it replaces the differentiation of $\phi_{\rm e}$ by the integration of $\mathbf{E}_{\rm t}$. In the standard FEM implementation of the Maxwell problem solver, the electric field is represented using the H(curl) elements. With this basis function, $D_{\rm n}$ is not a continuous function, which makes it difficult to evaluate the gradient accurately. Although a rigorous convergence analysis of the new iteration scheme is not yet performed, we believe eliminating the gradient operation is advantageous to minimize a numerical noise. Note that imposing $D_{\rm n}$ is not a natural form of BC in the boundary value problem of the Maxwell's equations. Therefore, we transformed it to a condition for the tangential magnetic field by introducing auxiliary scalar potentials and a Poisson equation [11]. We performed benchmark simulations using all relevant 2D simulations discussed in Ref. [33, 34, 35], which showed the excellent agreement in most of cases [37, 38]. Furthermore, in the RF SciDAC project, extensive code benchmark efforts of RF sheath models are made for the cross-verification of different implementations [39] and will be published in the future.

Although our sheath BC integration can handle non-linear sheath impedance and is tested with previous literature, a non-linear simulation with a realistic 3D antenna geometry is rather costly. At the moment, we are using this RF sheath potential model with a realistic tokamak antenna geometry in the so-called thick sheath limit (or asymptotic limit). The detail of this limit is discussed in Ref. [28]. In our non-linear iteration algorithm, this limit can be obtained by performing the first iteration of the non-linear loop with $D_{\rm n} = 0$ as the initial condition [11]. In FIG. 9 and 10, we show our initial application to the side limiters of the WEST ICRF antenna. In this simulation, we used a WEST ICRF antenna 3D model generated from the CAD geometry (FIG. 9) and imposed the RF sheath BC on the inner and outer sides of two poloidal side limiters. The rest of exterior boundaries are treated as the perfect electric conductor (PEC). Note that the limiter surface directly facing to the main plasma, where the magnetic field is nearly tangent to the surface, is treated as PEC as well (enlarged view in the FIG 9). The edge density is chosen to be $3 \times 10^{17}\mathrm{m}^{-3}$, which is much larger than the lower hybrid resonance density ($\sim 3 \times n_{\rm res}$), while a parabolic density profile with the central density of $4 \times 10^{19}\mathrm{m}^{-3}$ is used inside the last closed flux surface. As for the magnetic field profile, an equilibrium profile with the central magnetic field 3.5 T is used. As mentioned earlier, we use the cold plasma approximation even in the core region and enhance collisions, in order to mimic a strong single pass power absorption.

FIGURE 10 shows the computed RF sheath potential ($|\phi_{\rm e}|$), when 1 MW of ICRF power was injected. It can be seen that the sheath potential tends to concentrate near the top and bottom regions of the inboard side of limiters. Interestingly, the predicted sheath potential is in the range of 100 - 200V, suggesting that the RF sheath could be indeed a physics mechanism relevant to the ICRF-induced impurities. In Ref. [40] (FIG. 4a), the RF sheath activity localized to the top and bottom part of limiters is conjectured based on the IR camera and visible spectroscopy signals. Therefore, our results seem to be consistent with what is observed in the experiment, although the simulation setting needs to be refined in order to make a more direct comparison. Note that $|\phi_{\rm e}|$ is not exactly the same as the DC sheath potential, although they are tightly related. Our next step is to solve a global DC circuit equation in the similar way as discussed in Ref [28] and to evaluate the DC sheath potential profile on PFCs.

SUMMARY AND FUTURE DIRECTION

In order to better understand the RF actuator and improve its performance, we are advancing the computational modeling towards an integrated whole-device class RF actuator simulation. We took the approach to combine progresses made by various open source scientific and math software communities for meshing, FEM assembly, and linear solvers. Based on these open-source software libraries, we developed a self-contained FEM fullwave simulation platform (Petra-M). Recent progress in those computing software and hardware allows for resolving the HHFW wave field in a full 3D NSTX-U torus.

Verification and validation of the RF wave field computed by Petra-M has been a major research focus, which has been performed through the international/multi-institutional efforts. Careful comparison with RF antenna codes

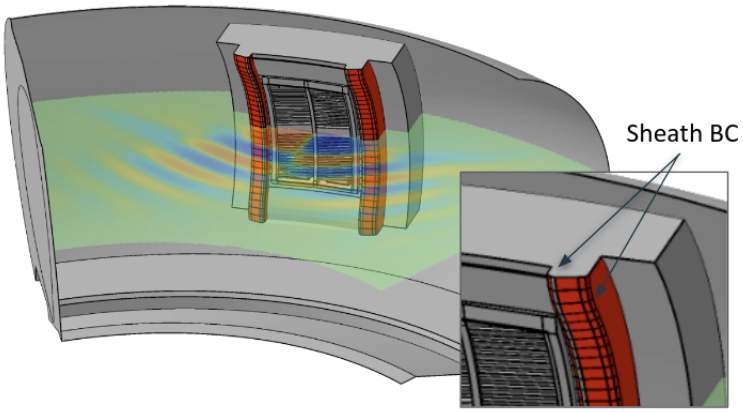

FIGURE 9. RF sheath boundary setting for WEST ICRF antenna. 60 degree sector of the WEST torus is simulated. The sheath BC is applied to the inboard and outboard side of side limiters indicated in red.

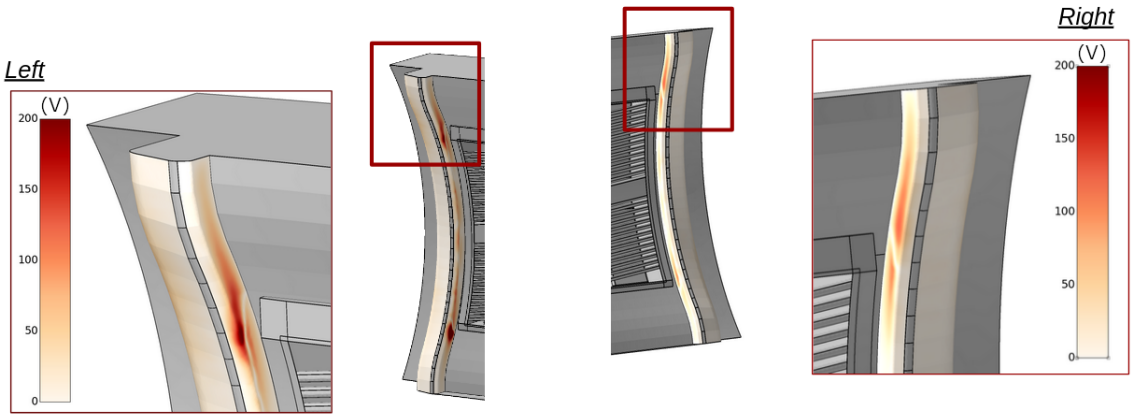

FIGURE 10. Profile of the RF sheath potential (ϕ_e) on the WEST ICRF antenna side limiters.

widely used in the community (RAPLICASOL and TOPICA) has been performed on various devices including AUG, JET and ITER, showing an excellent agreement in general. Furthermore, we interrogated deeply the computed 3D wave field using a spectral analysis technique, which shows that the wave field pattern is consistent with what is anticipated from the RF wave theory. On WEST, the LH wave excitation is computed using the entire LH1 antenna geometry, and the comparison with the DSELF diagnostic data is underway.

A significant progress has been made, in order to incorporate the RF sheath boundary conditions into 3D global wave field simulations. A new non-linear iteration scheme allows for using such a boundary condition with a Maxwell problem solver, which uses the de-facto standard H(curl) elements. The scheme was extensively tested with various 2D simulations and also verified in 3D in the thick sheath limit. The 3D RF sheath simulation on the WEST ICRF antenna indicates that the sheath potential tends to concentrate near the corner of antenna box, consistent with experimental observation of RF induced heat load pattern.

These progress discussed here started to reveal where and how knowing the 3D wave field is important. The HHFW simulations on NSTX-U show that the wave field at low n_ϕ components is launched from off-midplane parts of the antenna. As far as authors are aware, such an antenna excitation pattern was not considered in 2D simulations using TORIC, AORSA, and their equivalent, illustrating the importance of core-edge integrated wave field simulation. Throughout this paper, we approximated the plasma response to the RF using the cold plasma and collisions. Previously we discussed an approach to integrate TORIC core and FEM edge simulations self-consistently [1]. While the coupling algorithm itself easily extends to 3D, it requires to include a very large number of modes in 3D and we are still testing its feasibility using the WEST ICRF antenna.

Looking again at FIG. 1, our current status towards the integrated 3D RF simulation can be summarized as follows. The physics codes for components shown in the FIGURE are well established, and the algorithm to handle the physics interactions indicated by bi-directional arrows (1) to (3) are being developed. Our next step is to continue the model validation through various ICRF experiments worldwide, and at the same time, to switch gears more towards physics integration.

ACKNOWLEDGMENTS

This work was supported by the U.S. Department of Energy under contract number DE-AC02-09CH1146. The United States Government retains a non-exclusive, paid-up, irrevocable, world-wide license to publish or reproduce the published form of this manuscript, or allow others to do so, for United States Government purposes. This research also used resources of the National Energy Research Scientific Computing Center (NERSC), a U.S. Department of Energy Office of Science User Facility located at Lawrence Berkeley National Laboratory, operated under Contract No. DE-AC02-05CH11231.

REFERENCES

1. Shiraiwa S *et al.* 2017 *Nucl. Fusion* **57** 086048
2. Meneghini O *et al.* 2011 *AIP conf. Proceedings* **1406** 411
3. Smithe D *et al.* 2020 *AIP conf. Proceedings* **2254** 060009
4. Jenkins T, Smithe D *et al.* "modeling rf-induced ponderomotive effects on edge/sol transport: Nstx and beyond" *24th Topical Conference on Radio-frequency Power in Plasmas*
5. Shiraiwa, S *et al.* 2017 *EPJ Web Conf.* **157** 03048
6. Bertelli N *et al.* 2020 *AIP Conference Proceedings* **2254** 030001
7. Jacquot J *et al.* 2015 *AIP Conference Proceedings* **1689** 050008
8. Tierens W *et al.* 2019 *Nucl. Fusion* **59** 046001
9. Lancellotti D *et al.* 2006 *Nucl. Fusion* **46** S476
10. Milanesio D *et al.* 2009 *Nucl. Fusion* **49** 115019
11. Shiraiwa S *et al.* 2023 *Nucl. Fusion* **63** 026024
12. Migliore C *et al. Submitted to AIP conf. proceedings*
13. Beers C J *et al.* 2021 *Phys. Plasmas* **28**
14. MUMPS: a parallel sparse direct solver `http://mumps.enseeiht.fr/`
15. Open CASCADE Technology `https://www.opencascade.com/open-cascade-technology/`
16. pythonocc-core `https://github.com/tpaviot/pythonocc-core`
17. Bertelli N, Shiraiwa S and Ono M 2022 *Nucl. Fusion* **62** 126046 URL `https://dx.doi.org/10.1088/1741-4326/ac9690`
18. Tierens W *et al.* 2021 *ITER ICRH workshop*
19. Shiraiwa S *et al.* 2021 *47th EPS Conference on Plamsa Physics* **P5.1047**
20. Bertelli N *et al.* 2021 *47th EPS Conference on Plamsa Physics* **P2.1047**
21. Bertelli N *et al. Submitted to AIP conf. proceedings*
22. Milanesio D *et al.* "recent analysis of the iter ion cyclotron antenna with the topica code" *24th Topical Conference on Radio-frequency Power in Plasmas*
23. Milanesio D *et al.* "recent modeling for the iter ion cyclotron range of frequencies antennas with the topica code" submitted to NF
24. Tierens W *et al.* "icrf code benchmarks for the iter antenna; first non-axisymmetric cases" to be submitted to NF
25. Martin E *et al.* 2019 *Nucl. Fusion* **59** 076006
26. Myra J R 2021 *J. Plasma Phys.* **87** 905870504
27. Myra J R and D'Ippolito D A 2009 *Plasma Phys. Control. Fusion* **52** 015003
28. Colas L *et al.* 2012 *Phys. Plasmas* **19** 092505
29. Jacquot J *et al.* 2014 *Phys. Plasmas* **1** 061509
30. Kohno H, Myra J R and D'Ippolito D A 2015 *Phys. Plasmas* **22** 072504. **Erratum**: Phys. Plasmas **23** 089901, 2016.
31. Myra J R and D'Ippolito D A 2015 *Phys. Plasmas* **22** 062507
32. Colas L *et al.* 2017 *Plasma Phys. Control. Fusion* **59** 025014
33. Kohno H and Myra J R 2017 *Comp. Phys. Comm.* **220**
34. Kohno H and Myra J R 2019 *Phys. Plasmas* **26** 022507
35. Tierens W, Urbanczyk G, Colas L and Usoltceva M 2019 *Phys. Plasmas* **26** 083501
36. Jacquot J 2013 *Self-consistent non-linear description of radio-frequency wave propagation and of the edge of a magnetized plasma* Ph.D. thesis Université de Lorraine (France)
37. Shiraiwa S and Bertelli N 2022 Non-linear rf rectified sheath based on magnetic scalar potentials in petra-m *64th Annual Meeting of the APS Division of Plasma Physics,* URL `https://meetings.aps.org/Meeting/DPP22/Session/PP11.70`
38. Bertelli N *et al.* 2022 Benchmark of the linear and non-linear rf rectified sheath boundary conditions implemented in the petra-m fem platform

with the previous results obtained with the rfsol code *64th Annual Meeting of the APS Division of Plasma Physics,* URL `https://meetings.aps.org/Meeting/DPP22/Session/PP11.71`
39. Wright J C *et al.* 2021 Development of a non-linear rf sheath benchmark suite, *63rd Annual Meeting of the APS Division of Plasma Physics,* URL `https://meetings.aps.org/Meeting/DPP21/Session/GP11.10`
40. Urbanczyk G *et al.* 2021 *Nuclear Materials and Energy* **26** 100925